Ultrafast Control of Magnetic Anisotropy by Resonant Excitation of 4f Electrons and Phonons in $Sm_{0.7}Er_{0.3}FeO_3$

Gabriel Fitzky,[1] Makoto Nakajima,[2] Yohei Koike,[2] Alfred Leitenstorfer,[1] and Takayuki Kurihara[1,3,*]
[1]Department of Physics and Center for Applied Photonics, University of Konstanz, D-78457 Konstanz, Germany
[2]Institute of Laser Engineering, Osaka University, 2-6 Yamadaoka, Suita, Osaka, 565-0871, Japan
[3]Institute for Solid State Physics, The University of Tokyo, 5-1-5 Kashiwanoha, Kashiwa, Chiba, 277-8581, Japan

(Received 21 February 2021; accepted 28 July 2021; published 1 September 2021)

We compare the ultrafast dynamics of the spin reorientation transition in the orthoferrite $Sm_{0.7}Er_{0.3}FeO_3$ following two different pumping mechanisms. Intense few-cycle pulses in the midinfrared selectively excite either the f-f electronic transition of Sm^{3+} or optical phonons. With phonon pumping, a finite time delay exists for the spin reorientation, reflecting the energy transfer between the lattice and 4f system. In contrast, an instantaneous response is found for resonant f-f excitation. This suggests that 4f electronic pumping can directly alter the magnetic anisotropy due to the modification of 4f-3d exchange at femtosecond timescales, without involving lattice thermalization.

DOI: 10.1103/PhysRevLett.127.107401

Magnetic properties of correlated spin systems emerge as a result of complex interactions between spin, lattice, and electronic degrees of freedom. When subjected to intense electromagnetic fields, the magnetic order can be dynamically modified through various processes such as free-carrier injection [1], phonon excitation [2], ultrafast heating [3,4], Zeeman interactions [5–8], or stimulated Raman scattering [9,10]. Photoexcitation by continuous-wave and nanosecond lasers extends over timescales which are long as compared to typical processes for heat transfer between subsystems. Instead, femtosecond pulsed excitation and probing enables the distinction between purely electronic processes far from equilibrium and thermal dynamics involving the crystal lattice.

Transition metal magnets that contain rare-earth ions such as the orthoferrites ($RFeO_3$, R = rare earth) are typical examples wherein such complex couplings between subsystems determine the magnetic properties. In these materials, the magnetic anisotropy is defined by the exchange interaction between the 3d electron of the transition-metal ion and the 4f orbital of the rare-earth system because of the highly anisotropic shape of the latter [11,12]. It was pointed out theoretically in the 1980s that resonant photoexcitation of the 4f electronic system of the rare-earth ions might allow modification of magnetic anisotropy, offering a nonthermal route to ultrafast control of the macroscopic magnetization [13–16]. This idea was first tested successfully in $ErCrO_3$ using nanosecond laser excitation [13,14], showing that resonant pumping at f-f transition of Er^{3+} triggers a spin-reorientation transition (SRT) on microsecond time-scales. Still, lacking temporal resolution, the question remained whether the process happens in a purely electronic way or by assistance of heat transfer involving the lattice. Clarifying this question is central for determining the intrinsic time-scales for switching the SRT. Therefore, it is crucial to study the spin dynamics in the pico- to femtosecond time-scale, i.e., before the thermalization of 4f electrons with the surrounding lattice occurs. Simultaneously, the spin dynamics initiated by f-f transitions must be compared directly to ultrafast lattice heating. While the importance of such experiments has been evoked recently [8,16], direct femtosecond experiments on magnetic anisotropy control by resonant pumping of f-f transitions have been still lacking. Instead, the ultrafast SRT dynamics following femtosecond interband excitations and subsequent phonon heating has been studied extensively [4,17,18].

In this Letter, we independently excite the rare-earth electronic transitions and optical phonons, by using the intense femtosecond pulses in the midinfrared (MIR). The ultrafast dynamics of the SRT in the orthoferrite $Sm_{0.7}Er_{0.3}FeO_3$ is induced by pumping the f-f transition of the Sm^{3+} ion located at 33 THz, and is compared systematically with the case of ultrafast heat injection by optical phonons at 25 THz [Fig. 1(a)]. Analyzing the initial phase of the SRT dynamics shows an almost instantaneous change of magnetic anisotropy upon MIR irradiation in the case of resonant f-f pumping. In contrast, for phonon pumping a delay of approximately 3 ps is observed before SRT takes place, due to the finite energy transfer time from the lattice to the 4f electrons. Our results show that the magnetic anisotropy dominated by 4f-3d exchange can be controlled directly by the f-f resonant photoexcitation on time-scales much shorter compared to lattice thermalization or the SRT dynamics itself.

Orthoferrites $RFeO_3$ are weak ferromagnets, wherein antiferromagnetically ordered spins of Fe^{3+} 3d electrons are slightly canted due to Dzyaloshinskii-Moriya

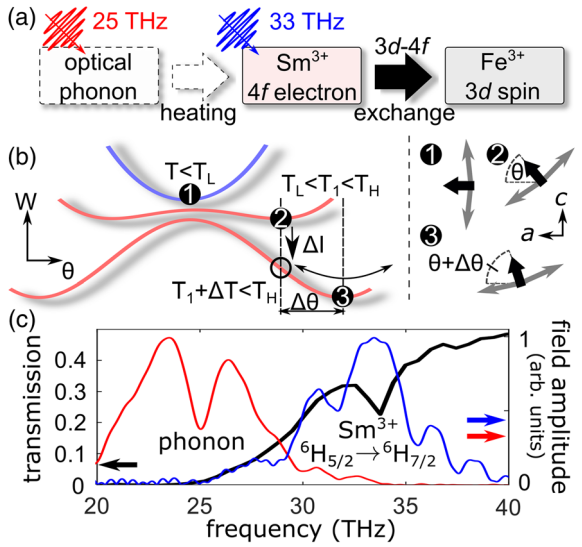

FIG. 1. (a) Schematic of magnetic anisotropy modulation by selective excitation of phonons or Sm^{3+} $4f$ electronic states by intense MIR. (b) Schematic of second-order SRT in the phenomenological anisotropy potential landscapes W at different lattice temperatures, indicating equilibrium spin positions below T_L (1), in the transition temperature before (2), and after MIR pumping (3).θ is the angle between the spin direction and the a axis of the crystal. (c) Transmission spectrum of $Sm_{0.7}Er_{0.3}FeO_3$ obtained by Fourier-transform infrared spectroscopy (black), and MIR pump spectra (red and blue) used in this work.

interaction and form a macroscopic magnetization $\boldsymbol{M}$. The magnetic properties are characterized by SRT, where the easy axis of magnetization changes from one axis to another with temperature due to modification of magnetic anisotropy [Fig. 1(b)] [19]. This effect originates from the exchange interaction between ferric $3d$ and rare-earth $4f$ electrons [12,20]. When temperature is increased, the paramagnetic moment of the $4f$ system decreases due to repopulation inside the crystal- and spin-orbit split states, thus reducing the $4f$-$3d$ exchange coupling. The unbalancing of the effective anisotropy of $3d$ spins along different crystal axes changes the shape of the anisotropy potential, reorienting the magnetic easy axis. Note that the local magnetic field set by the surrounding domains slightly favors one of the two energetic minima in Fig. 1(b), defining a preferred spin direction within the probe spot. No external magnetic bias is applied during the measurement to avoid affecting the SRT temperature [21]. We study a 50-μm-thick, c-cut single crystal sample of $Sm_{0.7}Er_{0.3}FeO_3$. It exhibits second-order SRT near room temperature ($\boldsymbol{M}\|a$ for $T < T_L = 310$ K and $\boldsymbol{M}\|c$ for $T > T_H = 330$ K) [22]. Sm^{3+} ions constitute isolated f-f resonance ($^6H_{5/2} \rightarrow {}^6H_{7/2}$) at 33 THz in a transparent window of the MIR region [Fig. 1(c)]. The narrow absorption linewidth attests to a weak electron-phonon coupling. Therefore, we expect that pumping with an intense MIR pulse centered at 33 THz selectively excites the $4f$ electrons without perturbing the lattice system. Compared to near-infrared and visible pump frequencies, the low photon energies of MIR pulses also come with minimum multiphoton absorption and unwanted excess heating of the electronic system. In contrast, the reststrahlen band of $Sm_{0.7}Er_{0.3}FeO_3$ sets in around 25 THz. Pumping in this frequency window should result in pure lattice excitation. We pump the system separately at these two transition frequencies [23], and probe the induced c-axis magnetization by the polarization change of the transmitted NIR pulses [24].

The time evolution of the Faraday ellipticity measured around the SRT temperature range is plotted in Fig. 2 for pump frequencies of 25 THz (left) and 33 THz (right), respectively. T_S indicates the target temperature of the substrate. The waveforms have several features in common. First, a sharp peak appears due to the birefringence caused by the nonresonant $\chi^{(3)}$ optical nonlinearity of the sample, defining the temporal origin $t = 0$. Subsequently, a strongly temperature-dependent dynamics follows which we attribute to spin reorientation. Above approximately 311 K for 25 THz pumping and 312 K for 33 THz, the signal gradually increases within a timescale of tens of picoseconds after MIR excitation, followed by an exponentially decaying oscillation. Thereafter, the signal settles to a finite value which lasts longer than the available time window of several nanoseconds limited by our mechanical delay stage.

The overall behavior of the transients may be understood qualitatively by ultrafast changes of the anisotropy potential following photoexcitation [Fig. 1(b)] [25,26]. Here, the phenomenological anisotropy potential landscapes W are sketched with respect to the angle θ between the spin direction and the a axis of the crystal for different effective temperatures. At temperatures sufficiently below T_L [scenario (1) in Fig. 1(b)], the potential features a single minimum at the a axis. Consequently, the magnetization direction is insensitive to the MIR-induced effective temperature change. In contrast, in the SRT region $T_L < T < T_H$, the potential exhibits two minima on opposite sides of the a axis [scenario (2), Fig. 1(b)]. Here, MIR excitation raises the effective temperature T_{eff} and shifts the potential minima away from the a axis. This effect causes the spin to precess toward the new minimum, resulting in the damped oscillation of the c-axis magnetization component. Finally, this motion settles to a new equilibrium position where the magnetization is slightly tilted toward the c axis [scenario (3), Fig. 1(b)]. Since the anisotropy strongly softens at $T = T_L$, the amplitude of the induced offset maximizes around this temperature.

To investigate the differences between spin dynamics induced by phonon- and f-f resonance excitations in more detail, we now quantitatively analyze the data based on the

inertial spin dynamics model [25,26]. We start from the Lagrangian and Rayleigh function of antiferromagnetic spins. Assuming that the MIR-induced change of the $3d$-$4f$ coupling and spin direction $\Delta\theta$ are sufficiently small, the Lagrangian equation of motion for the spin angle θ reduces to $\Delta\ddot{\theta} + 2\Gamma\Delta\dot{\theta} + \omega_0^2\Delta\theta = k\Delta T_{\mathrm{eff}}(t)$ [24]. Here, Γ represents damping, ω_0 the resonance frequency, ΔT_{eff} the effective temperature change, and k its coefficient. We model the temporal evolution of $\Delta T_{\mathrm{eff}}(t)$ as the sum of an exponentially increasing function and a delta function to account for both slow and fast thermalization dynamics, respectively: $k\Delta T_{\mathrm{eff}}(t) = A(1 - e^{-t/d}) + B\,\delta(t)$. Solving this equation analytically, we obtain the following expression for the limit of clearly underdamped oscillations:

$$\Delta\theta(t) = a(1 - e^{-t/d})\left[-1 + e^{-t/\tau}\cos(ft) + \frac{1}{f\tau}e^{-t/\tau}\sin(ft)\right] + be^{-t/\tau}\sin(ft). \quad (1)$$

Here, a describes the induced offset of spin angle in the final state relative to $t < 0$, τ the oscillation lifetime, f the oscillation frequency, d the effective rise time of ΔT_{eff}, and b the amplitude of the oscillation component arising from the delta-function force, respectively. The case of overdamping where f is close to zero is discussed later.

The thin black lines in Fig. 2 result from least-square fits based on Eq. (1), showing excellent agreement with experiment. The temperature dependence of each parameter extracted by fitting is plotted in Fig. 3. Data points connected by the black and blue lines represent the cases for 25 and 33 THz excitation, respectively. A noticeable difference between the two excitation cases is the relative shift of temperature with respect to each other. This effect is especially distinct in the oscillation frequency $f(T)$ and induced offset $a(T)$. It is attributed to the difference in stationary heating between the two pump frequencies inside the probed spot. Different absorption coefficients at 25 and 33 THz [Fig. 1(c)] translate directly to a slight offset in heat accumulation persisting over a timescale longer than the interpulse distance of 1 ms [24]. To provide detailed and quantitative comparison of the spin dynamics, we therefore shift the original 25 THz traces by +1.5 K, resulting in the red graphs in Fig. 3. The value of the temperature shift was chosen such that the oscillation frequencies $f(T)$ match the 33 THz case. Since $f(T)$ exhibits a strong temperature dependence reflecting the anisotropy softening [4], it provides a precise measure for the local temperature of the probed spot including stationary heating. In the following, we refer to these corrected data whenever any parameter for 25 THz is discussed. After this correction, the temperature dependence of the induced offset $a(T)$ evolves similarly for the two excitation cases. The behavior is consistent with previous reports in similar orthoferrites such as $ErFeO_3$ [17] and $TmFeO_3$ [4,17,18],

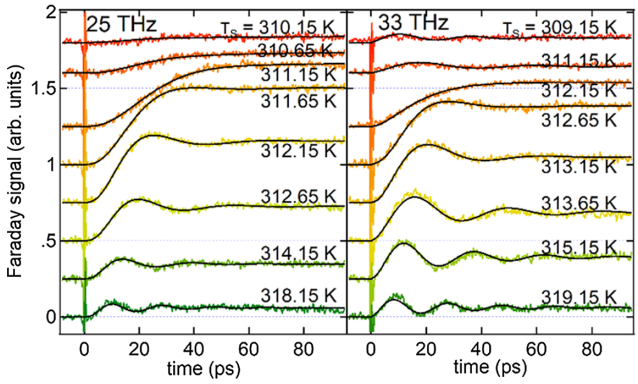

FIG. 2. MIR-induced Faraday ellipticity as a function of time delay at various substrate temperatures T_S in the SRT regime, pumped by 25 THz (left) and 33 THz (right) pulses. Solid black lines represent least-square fits to Eq. (1).

and clearly indicates the occurrence of SRT. It should be noted that despite the large difference of absorption coefficient between 25 and 33 THz [Fig. 1(c)], the magnitude of $a(T)$ is comparable in the two pumping cases. This finding indicates that the $4f$ electronic excitation modifies magnetic anisotropy more efficiently than phonon pumping.

In contrast to $a(T)$ and $f(T)$, the parameters $\tau(T)$, $d(T)$, and $b(T)$ evolve distinctly different for the two excitation cases. First, the oscillation lifetime $\tau(T)$ is significantly longer for 33 THz excitation (approximately 30 ps) compared to that of the 25 THz pulse (approximately 20 ps) in most of our temperature range. We neglect temperatures close to T_L (311.5 to 312.5 K) since our analytical solution [Eq. (1)] becomes invalid due to overdamping so the oscillation frequency and damping are unreliable. The shorter lifetime following 25 THz excitation is ascribed to spatial decoherence of the oscillation. Because of the strong absorption below 25 THz, MIR pulse powers near the front and the exit surface of the sample are expected to differ significantly. Because the oscillation frequency $f(T)$ depends strongly on transient temperature, the integration of the signal over the sample thickness by the probe pulse leads to an inhomogeneous decrease of the oscillation lifetime.

Next, we focus on parameter $d(T)$ representing the effective rise time of the anisotropy change. In the temporal waveforms, it appears as the delay time of the onset of the SRT dynamics after MIR excitation. $d(T)$ shows a qualitatively different temperature dependence in the two excitation cases. First, the 25 THz signal has a fairly large value of tens of picoseconds below T_L, while it continuously drops toward higher temperature. The presence of such large delay times is similar to previously reported laser-induced SRT dynamics of $ErFeO_3$ [17]. It has been suggested that even if the laser excitation heats up the lattice immediately, the relatively weak electron-phonon coupling between the phonon- and the $4f$-electronic system

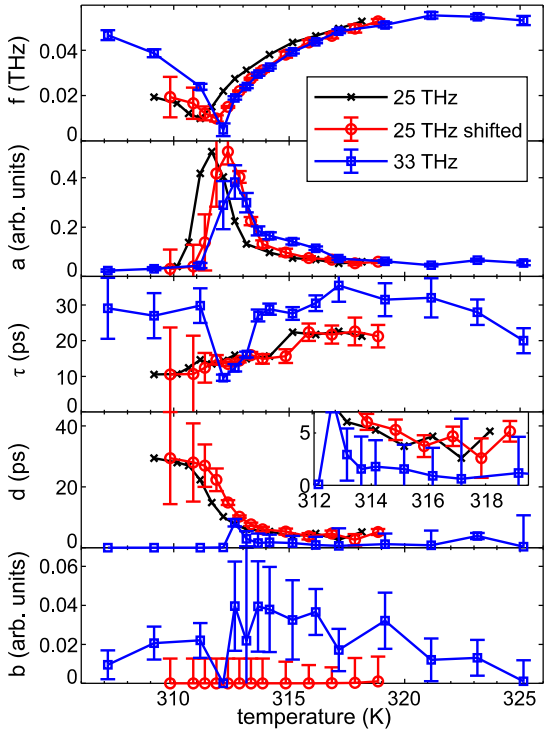

FIG. 3. Temperature dependence of the parameters obtained from least-square fits to the observed waveforms. Black crosses: originally measured 25 THz data without temperature correction; red circles: 25 THz data shifted by 1.5 K to account for stationary heating of the sample; blue squares: 33 THz excitation. Error bars show 95% confidence interval.

limits the energy transfer time. Consequently, the SRT dynamics initiates only after the effective $4f$-electronic temperature reaches T_L. Therefore, the lower the initial temperature, the longer it takes for the $4f$ system to reach T_L. This model is consistent with our observations below T_L in the case of 25 THz excitation. In contrast to $T < T_L$, d settles to a constant value of approximately 3–5 ps inside the SRT region (inset of d in Fig. 3). Based on the same argument, we assume that this value directly reflects the lattice-$4f$ thermalization time.

The behavior of $d(T)$ in the 33 THz excitation case strongly differs from the one at 25 THz. Here, d is much smaller at each temperature, typically below 1–2 ps (inset Fig. 3). This discrepancy is also observable directly in the original temporal waveforms highlighted in Fig. 4. At each temperature below (a) and above (b) and (c) T_L, the Faraday signal starts to increase immediately after the excitation by 33 THz pulses. The 25 THz excitations, however, always feature a finite delay until the Faraday signal increases. This behavior indicates that upon resonant f-f pumping, the slow thermalization dynamics of the lattice is not involved and the magnetic anisotropy is immediately modified. We understand the underlying mechanism of this process in the following manner: when the 33 THz pump pulses induce the ${}^6H_{5/2} \rightarrow {}^6H_{7/2}$ transition, the angular momentum of each photoexcited Sm^{3+} ion changes as $J = 5/2 \rightarrow 7/2$. We estimate that around 0.5% of the total Sm^{3+} ions in the pump volume are excited [24]. The change in angular momentum immediately alters the $4f$-$3d$ exchange interaction with the Fe^{3+} spins, resulting in the instantaneous modification of the magnetic anisotropy. Because the transition occurs on the timescale of tens of femtoseconds ($1/33$ THz ~ 30 fs), it is conceivable that the $4f$-$3d$ exchange modification takes place within a similarly short timescale.

Strong evidence for ultrafast anisotropy modification beyond the thermalization time in the case of f-f excitation is found in parameter $b(T)$ in Fig. 3. It represents the component of the MIR-induced anisotropy change expressed by the delta-function force in Eq. (1). In case of 25 THz, the values of b are negligible throughout the entire temperature range, while they remain finite for 33 THz pumping. The presence of this component is also seen directly in the initial spin dynamics imprinted into the temporal waveform of Fig. 4(c). Immediately after pumping at $t = 0$, the Faraday signal increases linearly. This observation indicates that the driving force of the induced spin dynamics is indeed impactlike: When such a force is applied to a harmonic oscillator, it acquires finite *velocity* so the position increases linearly with a finite gradient after the excitation. On the other hand, if the applied force consists of a step function, it provides an *acceleration* to the harmonic oscillator which results in the *quadratic* signal increase. The initial behavior of the measured 33 THz excitation waveform from $t = 0$ to $t = 5$ ps [Fig. 4(c)] clearly matches the former dynamics rather than the latter. Therefore, our observation confirms that the resonant excitation of f-f transition by femtosecond MIR transients rapidly modifies the magnetic anisotropy at ultrafast timescales far below that of both the lattice heating and the SRT itself, which takes several tens of picoseconds.

The existence of the delta-function force in addition to the onset of the MIR-induced anisotropy change is understood from the electronic population dynamics of the photoexcited Sm^{3+} $4f$ ion. It was suggested previously [16,32–34] that due to the $4f$-$3d$ coupling, the excited Sm^{3+} ion transfers energy to the Fe^{3+} $3d$ states within 3–4 ps. Subsequently, the $3d$ state thermalizes with the lattice, resulting in a new thermal equilibrium between the three subsystems. The former dynamics effectively serves as a delta function force on the spin system, while the latter results in the long-lasting offset represented by the step function in our model.

To conclude, we compared the ultrafast spin reorientation dynamics in $Sm_{0.7}Er_{0.3}FeO_3$ induced by resonant electronic excitation of the f-f transition of the Sm^{3+} $4f$ system at 33 THz and phonon pumping at 25 THz. Under resonant f-f pumping, the SRT dynamics immediately starts upon photoexcitation without the initial time delay that is characteristic to the case of ultrafast lattice

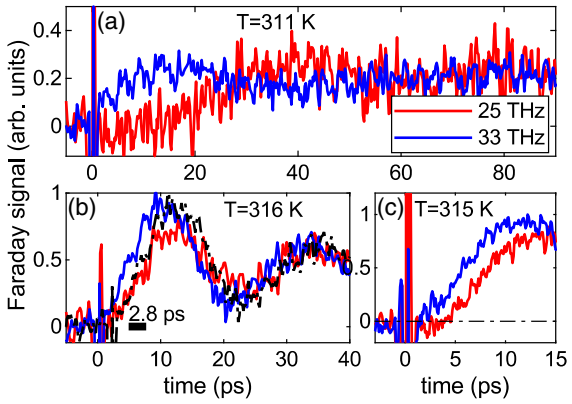

FIG. 4. Comparison of initial dynamics of spin reorientation between 25 THz (red) and 33 THz (blue) pumping at temperatures of 311 K (a), 316 K (b), and 315 K (c). The black dashed graph in (b) represents the 33 THz results temporally shifted by +2.8 ps.

heating. Energy transfer times from the lattice to the $4f$ system between 3 and 5 ps are identified. Furthermore, by analyzing the initial dynamics of the SRT induced by 33 THz excitation, we show that the $4f$ resonant pumping instantaneously modifies the anisotropy much faster than the spin dynamics itself, most likely at the few-femtosecond timescale. Our result demonstrates that in systems where $4f$-$3d$ exchange dominates the magnetic anisotropy, it can be modified electronically by ultrafast resonant pumping of the f-f transition without involving lattice thermalization. The selective f-f pumping scheme can be applied to many types of magnetic materials containing rare-earth ions to investigate how the $4f$ electronic state influences the magnetic properties. With further improvement of the time resolution, it will become attractive to apply this scheme to study the microscopic role of exchange interactions in the elementary dynamics of magnetic systems on a subcycle optical scale. This goal may be achieved by selectively probing specific electronic transitions of the Fe^{3+} ions that are sensitive to the $4f$-$3d$ coupling.

This work has been funded by the Deutsche Forschungsgemeinschaft (DFG, German Research Foundation) – SFB 1432 – Project-ID 425217212. T. K. is thankful for the support from Overseas Research Fellowship of the Japan Society for the Promotion of Science (JSPS), JSPS KAKENHI (JP20K22478, JP21K14550), and Zukunftskolleg Fellowship from the University of Konstanz. M. N. received support from JSPS KAKENHI (JP20H02206). This work was partly carried out by the joint research in the Institute for Solid State Physics, the University of Tokyo in the floating-zone growth of the $Sm_{0.7}Er_{0.3}FeO_3$ single crystal. G. F., M. N., and T. K. conducted the experiments. G. F. and T. K. analyzed the data and, together with A. L., wrote the manuscript. Y. K. and M. N. provided the sample. T. K. and M. N. designed the experiment. A. L. supervised the project together with T. K. All authors contributed to the discussion and reviewed the manuscript.

*Corresponding author.
takayuki.kurihara@issp.u-tokyo.ac.jp

[1] J. A. Gupta, R. Knobel, N. Samarth, and D. D. Awschalom, Science **292**, 2458 (2001).
[2] T. F. Nova, A. Cartella, A. Cantaluppi, M. Först, D. Bossini, R. V. Mikhaylovskiy, A. V. Kimel, R. Merlin, and A. Cavalleri, Nat. Phys. **13**, 132 (2017).
[3] T. A. Ostler *et al.*, Nat. Commun. **3**, 666 (2012).
[4] K. Yamaguchi, T. Kurihara, H. Watanabe, M. Nakajima, and T. Suemoto, Phys. Rev. B **92**, 064404 (2015).
[5] K. Yamaguchi, M. Nakajima, and T. Suemoto, Phys. Rev. Lett. **105**, 237201 (2010).
[6] T. Kurihara, H. Watanabe, M. Nakajima, S. Karube, K. Oto, Y. C. Otani, and T. Suemoto, Phys. Rev. Lett. **120**, 107202 (2018).
[7] T. Kampfrath, A. Sell, G. Klatt, A. Pashkin, S. Mährlein, T. Dekorsy, M. Wolf, M. Fiebig, A. Leitenstorfer, and R. Huber, Nat. Photonics **5**, 31 (2011).
[8] S. Baierl, J. H. Mentink, M. Hohenleutner, L. Braun, T.-M. Do, C. Lange, A. Sell, M. Fiebig, G. Woltersdorf, T. Kampfrath, and R. Huber, Phys. Rev. Lett. **117**, 197201 (2016).
[9] F. Hansteen, A. Kimel, A. Kirilyuk, and T. Rasing, Phys. Rev. B **73**, 014421 (2006).
[10] A. V. Kimel, C. D. Stanciu, P. A. Usachev, R. V. Pisarev, V. N. Gridnev, A. Kirilyuk, and Th. Rasing, Phys. Rev. B **74**, 060403(R) (2006).
[11] T. Yamaguchi, J. Phys. Chem. Solids **35**, 479 (1974).
[12] X. Li, M. Bamba, N. Yuan, Q. Zhang, Y. Zhao, M. Xiang, K. Xu, Z. Jin, W. Ren, G. Ma, S. Cao, D. Turchinovich, and J. Kono, Science **361**, 794 (2018).
[13] S. Kurita, K. Toyokawa, K. Tsushima, and S. Sugano, Solid State Commun. **38**, 235 (1981).
[14] S. Kurita, Y. Tazaka, and K. Tsushima, J. Phys. Soc. Jpn. **56**, 612 (1987).
[15] E. I. Golovenchits, V. A. Sanina, and T. A. Shaplygina, Zh. Eksp. Teor. Fiz. **80**, 1911 (1981), https://inis.iaea.org/search/searchsinglerecord.aspx?recordsFor=SingleRecord&RN=13704161.
[16] D. Bossini, D. Malik, B. Redlich, A. F. G. van der Meer, R. V. Pisarev, Th. Rasing, and A. V. Kimel, Phys. Rev. B **87**, 085101 (2013).
[17] J. A. de Jong, A. V. Kimel, R. V. Pisarev, A. Kirilyuk, and Th. Rasing, Phys. Rev. B **84**, 104421 (2011).
[18] A. V. Kimel, A. Kirilyuk, A. Tsvetkov, R. V. Pisarev, and T. Rasing, Nature (London) **429**, 850 (2004).
[19] G. F. Herrmann, Phys. Rev. **133**, A1334 (1964).
[20] A. I. Belyaeva and K. V. Baranova, Bull. Russ. Acad. Sci. Phys. **73**, 1056 (2009).
[21] T. Suemoto, K. Nakamura, T. Kurihara, and H. Watanabe, Appl. Phys. Lett. **107**, 042404 (2015).
[22] X. Zhao, K. Zhang, K. Xu, P. Man, T. Xie, A. Wu, G. Ma, S. Cao, and L. Su, Solid State Commun. **231–232**, 43 (2016).

[23] C. Schmidt, J. Bühler, A.-C. Heinrich, J. Allerbeck, R. Podzimski, D. Berghoff, T. Meier, W. G. Schmidt, C. Reichl, W. Wegscheider, D. Brida, and A. Leitenstorfer, Nat. Commun. **9**, 2890 (2018).

[24] See Supplemental Material at http://link.aps.org/supplemental/10.1103/PhysRevLett.127.107401 for details concerning the experimental setup, the detection scheme, the derivation of the inertial spin dynamics model leading to Eq. (1), transient heating, and number of excited Sm^{3+} ions, which includes Refs. [22,25–31].

[25] S. Baierl, M. Hohenleutner, T. Kampfrath, A. K. Zvezdin, A. V. Kimel, R. Huber, and R. V. Mikhaylovskiy, Nat. Photonics **10**, 715 (2016).

[26] A. V. Kimel, B. A. Ivanov, R. V. Pisarev, P. A. Usachev, A. Kirilyuk, and T. Rasing, Nat. Phys. **5**, 727 (2009).

[27] S. R. Woodford, A. Bringer, and S. Blügel, J. Appl. Phys. **101**, 053912 (2007).

[28] P. A. Usachev, R. V. Pisarev, A. M. Balbashov, A. V. Kimel, A. Kirilyuk, and T. Rasing, Phys. Solid State, **47**, 2292 (2005).

[29] A. J. Kurtzig, J. Appl. Phys. **42**, 3494 (1971).

[30] K. Saito, Y. Yamamura, J. Mayer, H. Kobayashi, Y. Miyazaki, J. Ensling, P. Gütlich, B. Leśniewska, and M. Sorai, J. Magn. Magn. Mater. **225**, 381 (2001).

[31] K. Persson, Materials data on $ErFeO_3$ (SG:62) by materials project, 2014, https://doi.org/10.17188/1200364.

[32] R. V. Mikhaylovskiy, T. J. Huisman, A. I. Popov, A. K. Zvezdin, Th. Rasing, R. V. Pisarev, and A. V. Kimel, Phys. Rev. B **92**, 094437 (2015).

[33] R. V. Mikhaylovskiy, T. J. Huisman, R. V. Pisarev, Th. Rasing, and A. V. Kimel, Phys. Rev. Lett. **118**, 017205 (2017).

[34] D. Afanasiev, A. K. Zvezdin, and A. V. Kimel, Opt. Express **23**, 23978 (2015).